



SiSTL2 Is Required for Cell Cycle, Leaf Organ Development, Chloroplast Biogenesis, and Has Effects on C₄ Photosynthesis in *Setaria italica* (L.) P. Beauv.

Shuo Zhang[†], Sha Tang[†], Chanjuan Tang, Mingzhao Luo, Guanqing Jia, Hui Zhi* and Xianmin Diao*

Institute of Crop Sciences, Chinese Academy of Agricultural Sciences, Beijing, China

OPEN ACCESS

Edited by:

Jianjun Chen,
University of Florida, United States

Reviewed by:

Xinguang Zhu,
University of Chinese Academy
of Sciences (UCAS), China
Taniguchi Mitsutaka,
Nagoya University, Japan

*Correspondence:

Hui Zhi
zhihui@caas.cn
Xianmin Diao
diaoxianmin@caas.cn

[†] These authors have contributed
equally to this work.

Specialty section:

This article was submitted to
Plant Breeding,
a section of the journal
Frontiers in Plant Science

Received: 26 February 2018

Accepted: 09 July 2018

Published: 30 July 2018

Citation:

Zhang S, Tang S, Tang C, Luo M,
Jia G, Zhi H and Diao X (2018) SiSTL2
Is Required for Cell Cycle, Leaf Organ
Development, Chloroplast
Biogenesis, and Has Effects on C₄
Photosynthesis in *Setaria italica* (L.) P.
Beauv. *Front. Plant Sci.* 9:1103.
doi: 10.3389/fpls.2018.01103

Deoxycytidine monophosphate deaminase (DCD) is a key enzyme in the *de novo* dTTP biosynthesis pathway. Previous studies have indicated that DCD plays key roles in the maintenance of the balance of dNTP pools, cell cycle progression, and plant development. However, few studies have elucidated the functions of the DCD gene in Panicoideae plants. *Setaria* has been proposed as an ideal model of Panicoideae grasses, especially for C₄ photosynthesis research. Here, a *Setaria italica* stripe leaf mutant (*sistl2*) was isolated from EMS-induced lines of “Yugu1,” the wild-type parent. The *sistl2* mutant exhibited semi-dwarf, striped leaves, abnormal chloroplast ultrastructure, and delayed cell cycle progression compared with Yugu1. High-throughput sequencing and map-based cloning identified the causal gene *SiSTL2*, which encodes a DCD protein. The occurrence of a single-base G to A substitution in the fifth intron introduced alternative splicing, which led to the early termination of translation. Further physiological and transcriptomic investigation indicated that *SiSTL2* plays an essential role in the regulation of chloroplast biogenesis, cell cycle, and DNA replication, which suggested that the gene has conserved functions in both foxtail millet and rice. Remarkably, in contrast to DCD mutants in C₃ rice, *sistl2* showed a significant reduction in leaf cell size and affected C₄ photosynthetic capacity in foxtail millet. qPCR showed that *SiSTL2* had a similar expression pattern to typical C₄ genes in response to a low CO₂ environment. Moreover, the loss of function of *SiSTL2* resulted in a reduction of leaf ¹³C content and the enrichment of DEGs in photosynthetic carbon fixation. Our research provides in-depth knowledge of the role of DCD in the C₄ photosynthesis model *S. italica* and proposed new directions for further study of the function of DCD.

Keywords: dCMP deaminase, chloroplast biogenesis, cell cycle, cell expansion, C₄ photosynthesis, *Setaria italica*

INTRODUCTION

Deoxycytidine monophosphate deaminase (DCD) is a key enzyme in the *de novo* deoxythymidine triphosphate (dTTP) synthesis pathway. DCD catalyzes the deamination of deoxycytidylate (dCMP) to produce deoxyuridine monophosphate (dUMP), the latter of which is the substrate that ultimately forms dTTP (Ellims et al., 1981). As described in previous studies, DCD contains two

conserved motifs, HXE and PCXXC, which reportedly function as a zinc-binding motif (Weiner et al., 1993). The DCD monomer is characterized to have between four and five α -helices and six β -sheets, which are arranged in an α - β - α sandwich (Scortecci et al., 2017). Six DCD monomers combine to form a biologically active homohexamer in bacteria and animals (Hou et al., 2008). As an allosteric enzyme, DCD contains an allosteric site. dTTP and deoxycytidine triphosphate (dCTP) are the inhibitor and activator of DCD, respectively, which competitively bind to the allosteric site to control protein stability and further regulate the activity of DCD (Hou et al., 2008; Marx and Alian, 2015). This allosteric regulation depends on the participation of divalent metal ions, such as Ca^{2+} and Mg^{2+} (Scortecci et al., 2017). The pools of dTTP and deoxyribonucleoside triphosphates (dNTPs) are basic elements essential for DNA synthesis, replication, recombination, and repair (Kumar et al., 2011), which further guarantee the normal procession of these biological pathways. Two enzymes, the abovementioned DCD and ribonucleoside reductase (RNR), are mostly responsible for the maintenance of sufficient dTTP (Ke et al., 2005). RNR, which catalyzes the reduction reaction to produce deoxy-ribonucleotide diphosphate (dNDPs), is responsible for the *de novo* biosynthesis of four dNTPs to ensure the dNTP pools balance (Buckland et al., 2014). In addition to the *de novo* pathway, dTTP can be supplemented by the thymidine kinase (TK) salvage pathway in a majority of higher eukaryotes. TK, as the key enzyme in the salvage pathway, can catalyze the phosphorylation of deoxidized thymidine to form deoxythymidine monophosphate, the substrate to produce dTTP (Leija et al., 2016). When either of the *de novo* or salvage pathway is defective, the other can compensate for the loss of pyrimidine synthesis function (Leija et al., 2016). Thus, these pathways are mutually interrelated to maintain sufficient dTTP and the balance of the dNTP pools. In addition, the biosynthesis of dTTP is a highly coordinated process.

Deoxycytidine monophosphate deaminase defects always lead to the imbalance of the dNTP pools and further cause the abnormal synthesis of DNA. In the process of DNA synthesis, the accuracy of DNA polymerase depends on the supply of dNTPs (Buckland et al., 2014). When the correct dNTP inserts into a nucleotide chain, it competes with three other kinds of dNTPs. In addition, the fidelity of DNA replication also depends on the GC% in the dNTP pools. Thus, unbalanced dNTP pools increase the probability of the insertion of the wrong base (Gu and Li, 1994; Gawel et al., 2014). In addition, unbalanced dNTP pools can increase the frequencies of insertion/deletion mutations (Kumar et al., 2011). It has been reported that in fission yeast, the deletion of *DCD1* leads to drastic changes in the accumulations of dCTP and dTTP. The mutant strain becomes sensitive to DNA damage inducers, has a decreased capacity for DNA replication and repair, even appears the collapse of replication fork (Sanchez et al., 2012). Previous studies also reported that in budding yeast, *DCD* or *RNR* mutation could increase the mutation rates, slow down the DNA replication, and impact the genome integrity and stability (Kohalmi et al., 1991; Sanchez et al., 2012). In rice, the mutation of *OsDCD* results in DNA damage and leaf cell apoptosis (Niu et al., 2017).

In contrast, DCD decrease sometimes impaired cell cycle progression. The S-phase is the period in which the majority of DNA replication is established. Thus, the adequacy of dNTPs is a precondition of entrance into S-phase (McIntosh et al., 1986). Insufficient dNTPs or the imbalance of dNTP pools can activate the S-phase checkpoint, delay the progress of the cell cycle, decrease the cell proliferation rate, and even lead to cell apoptosis (Kumar et al., 2010). Previous studies have established that DCD or RNR deficiency in yeast resulted in cell cycle arrest in the S-phase (Elledge and Davis, 1990; Sanchez et al., 2012). The deficits of DCD in rice also cause cell cycle progression defects (Niu et al., 2017). DCD and other dNTPs biosynthetic genes are coordinated with cell cycle progression. Some cell cycle associated enzymes participate in the regulation of nucleotide metabolizing genes (Ke et al., 2005). In addition, the activities of most dTTP synthetic enzymes exhibit periodic fluctuations during the cell cycle (McIntosh et al., 1986). TK and thymidylate kinase (TMPK) are the targets of the cell cycle proteasome APC/C and can be degraded by APC/C during the G1-phase to maintain the balance of the dNTP pools in mammals (Ke et al., 2005). E2Fs, as important cell cycle associated transcription factors (TFs), can induce specific *RNR1a* expression in the G1/S-phase (Lincker et al., 2004). However, *DCD1* is reported to have a periodic expression level during the cell cycle in HeLa cells, but is transcribed at a constant level in *Saccharomyces cerevisiae* (McIntosh et al., 1986).

In higher plants, mutations of dNTPs synthesis genes always result in abnormal leaf development. For example, the phenotype of the *Arabidopsis thaliana* *RNR1* mutant has crinkled leaves with white pits. The mutant has fewer, larger, and dysplastic chloroplasts (Garton et al., 2007). Similarly, mutations in large and small subunits of RNR in rice lead to dwarf plants, white stripe leaves, low chlorophyll contents, and undeveloped chloroplasts (Yoo et al., 2009; Qin et al., 2017). There are few reports on DCD gene functions in higher plants. A previous study showed that rice *OsDCD* mutant *st2* has white stripe leaves and reduced plant height. The chloroplast development and chlorophyll accumulation of *st2* are defected (Xu et al., 2014). In a recent study, another rice *DCD* mutant, *alr*, showed similar, but more severe phenotypes compared with *st2*, which had a small grain size and necrotic spots on the leaves. In addition, the cells of the *alr* mutant were increased in size, but decreased in number (Niu et al., 2017). Previous studies have proposed several explanations for these phenotypes in the *OsDCD* mutant. First, the unbalanced dNTP pools impaired the plastid genome replication and delayed chloroplast development. Second, the cell cycle progression and cell division were influenced, which resulted in small organs and dwarf plants (Niu et al., 2017).

Here, we isolated an *Setaria italica* mutant *sistl2* from EMS-induced lines of the Yugu1 cultivar. The mutant gene *SiSTL2* encodes a DCD protein. *sistl2* has similar phenotypes to those of *alr* and *st2* in rice. More interestingly, we found that *sistl2* was different to the rice *alr* mutant, including significantly reduced leaf cell size, normal second and third leaves, and uninfluenced grain size. It is worth noting that the C_4 photosynthetic character

of *sistl2* was affected, which has not been previously reported. In our study, we analyzed the mutant phenotypes, the expression of the causal genes, and expounded the function of *SiSTL2* in *S. italica*. Our research provides further insights into the role of DCD in the C_4 model *S. italica* and proposed new perspectives for further study of DCD functions.

MATERIALS AND METHODS

Plant Materials and Growth Condition

The *sistl2* mutant was obtained from the EMS-induced *S. italica* cultivar Yugu1. The identified mutant plants were backcrossed with Yugu1 three times before the characterization of the morphological and physical traits. To measure the agronomic traits and to determine the chlorophyll content and photosynthesis rate of Yugu1 and *sistl2*, the plants were grown in the experimental fields of the Institute of Crop Sciences, Chinese Academy of Agricultural Sciences, in Beijing (116.6° E, 40.1° N), China.

Chlorophyll Content, Photosynthetic Rate, and Chlorophyll Fluorescence

Setaria italica leaves harvested from the heading stage were cut into pieces and soaked in 95% alcohol for approximately 3 days until the leaf pieces were discolored completely. The supernatant was then collected and the absorbance values at 665 and 649 nm were measured by using a UV-1800 ultraviolet/visible light spectrophotometer. Chlorophyll *a* (Chl *a*) and chlorophyll *b* (Chl *b*) levels were then calculated by using the equation reported by Lichtenthaler (1987). The photosynthetic parameters were measured on fine mornings by using the Li-6400 portable photosynthesis system (LI-COR, Lincoln, NE, United States) to analyze mature leaves from five individual heading stage plants (6400-02B LED light source, ParIn = 1000 $\mu\text{mol m}^{-2} \text{s}^{-1}$). The $\Delta\Phi\text{PS II}$ [(Fm'–Fs)/Fm'] was calculated from the equation mentioned by Hu et al. (2014).

Phenotypic Analysis of Leaf Venation Patterns

The leaves gained from the heading stage were observed and photographed by using an AnytyTM 3R MSV500 portable digital microscope (3R Eddytek, Beijing, China). For the I₂-KI dye, the leaves were cut into pieces of 5 mm × 5 mm and fixed in FAA (3.7% formaldehyde, 50% ethanol, and 5.0% glacial acetic acid) overnight at 4°C, followed by a graded ethanol series and xylene series, and finally dyed in I₂-KI for 12 h. The samples were then observed and photographed by using a light microscope. For the cell size measurement, 20 medium-sized cells from three horizons were analyzed by using Image-Pro plus 6.0 (Media Cybernetics, Silver Spring, Georgia Avenue, United States).

Leaf Microstructure Observations

For the leaf cross section, the leaves of the seedling stage were cut into pieces of 2 mm × 1 mm, fixed, and treated as described above. After the treatment, the samples were embedded in

resin. Microtome sections were stained with toluidine blue and photographed by using a light microscope.

For transmission electron microscopy (TEM) analysis, the leaf materials were obtained from seedlings of Yugu1 and *sistl2* and cut into pieces of 2 mm × 1 mm. The materials were fixed overnight in 0.1 M phosphate buffer with 2.5% glutaraldehyde. Then the samples were washed three times with 0.2 M phosphate buffer and post-fixed in 1% osmium tetroxide for 1 h. After staining with uranyl acetate, the samples were further dehydrated in a gradient ethanol series and finally embedded into resin. Ultrathin sections were made and examined by using a JEM 1230 TEM.

Map-Based Cloning and High-Throughput Sequencing

For MutMap+ analysis (Fekih et al., 2013), the leaf samples were harvested from recessive individuals and dominant individuals, respectively. Then, two DNA pools contained the same amounts of DNA samples from 27 recessive/dominant individuals for whole genome resequencing were built. The resequencing was performed by using the Illumina HiSeq 2500 platform with a 150 bp paired-end strategy. The raw sequencing data was deposited at EMBL-EBI in the European Nucleotide Archive database under the accession number ERP106777. Data from the two sample pools were aligned to each other and analyzed in accordance with methods described in our previous study (Xiang et al., 2017).

To exclude irrelevant SNPs from the results of MutMap+ analysis, an F₂ population from the hybridization between *sistl2* and the SSR41 cultivar was used for mapping of the *SiSTL2* locus. Three SSR markers based on earlier studies (Jia et al., 2009; Zhang et al., 2014) were adopted and an In-Del marker Ins9-1 was designed for gene cross positioning (**Supplementary Table S1**). To verify the change in transcript splicing, coding sequences of *Setaria.9G511200* in WT and *sistl2* were amplified by using PCR primers (5'-ATGGCCTCGACGAGGGA-3' and 5'-AAGGGCAAGGGAGTGAT-3') and transformed into vectors by using the pEASY-Blunt cloning Kit (TRAN, Beijing, China). Four clones of each transformed cases were picked for sequencing by using the M13+/- universal primer.

Complementation Assay

The PCR reaction for the amplification of the promoter (primer with underlined in-fusion adaptor: 5'-GGCCAGTGCC AAGCTTCGTCGTTCCCTCCAAGTT-3' and 5'-TCGAGGCC ATGGATCCCGCGCTCGGGCGGTGGGGA-3') and genome sequence (primer with in-fusion adaptor underlined: 5'-CCCG AGCGCGGGATCCATGGCCTCGACGAGGGA-3' and 5'-GA TCGGGAAATTTCGAGCTCAGAGGATCAAGCCATAGGAC AC-3') of *SiSTL2* were performed and transformed into the pTCK303 vector by using the In-Fusion HD Cloning Kit (Cat no. 072012, Clontech, United States) in two separate operations. The rice *Ubiquitin* gene was used as a reference for the RT-qPCR of transgenic lines in accordance with a previous report (Wang Y. et al., 2017).

Bioinformatics Analysis

The sequence, structure, and function annotation of the candidate genes were obtained from the *S. italica* V2.2 database of *Phytozome*¹. The functional domains and motifs were predicted from the amino acid sequence by Conserved Domain search in *NCBI*². The 3D structure analysis was produced by the *PDB* database³. Transcription factor binding sites were predicted by PlantRegMap⁴.

Enzymatic Assays

For enzymatic assays, Wild-type *SiSTL2* cDNA and mutant *SiSTL2* cDNA (sequence before the mutant site) was subcloned into pCold vector and transformed into *E. coli* Transetta (DE3) for prokaryotic expression (sequences of primers with underlined in-fusion adaptor: for WT, 5'-TACCCTCGAGGGATCCATGGCCTCGACGAGGGA-3' and 5'-GCTTGAATTCCGATCCTGGCTCCTGAACTTGATCG-3'; for mutant, 5'-TACCCTCGAGGGATCCATGGCCTCGACGAGGGA-3' and 5'-GCTTGAATTCCGATCCTAGGATTATCCCTCTTGGCT-3'). Bacterial cultures (2 ml) were grown overnight at 37°C in LB medium, then transformed into 200 ml LB, and cultivate until OD₆₀₀ = 0.6. Then the cells were induced using 0.3 mM isopropyl β-D-thiogalactopyranoside (IPTG) for 10 h at 15°C. Next, the cells were harvested by centrifugation and resuspended in 1 × PBS buffer, containing 1 mM PMSF and 100 unit/ml DNase. After disruption by sonication, the cell debris was removed by centrifugation at 16,100 g for 10 min. The soluble lysis fraction was purified by histidine specific Ni-NTA agarose resin and the target protein was eluted in elution buffer. Finally, the wild-type and mutant fusion protein with histidine tag were detected by SDS-PAGE, and used in enzyme assays.

Enzyme assays were conducted to measure the specific activity at 30°C in the buffer described previously with 100 μM dCTP and 0.2 mM MgCl₂ (Hou et al., 2008; Niu et al., 2017) by detecting the decrease in absorption at 290 nm using a UV-1800 ultraviolet/visible light spectrophotometer. The dCMP concentration varied from 0 to 3 mM with a grade of 0.5 mM. The enzyme concentration was fixed at 0.5 μg/ml. All measurements were performed three times, and average values and standard deviation were calculated.

qRT-PCR Analysis

The total RNA was gained from fresh plant tissues by using a Pure Link RNA Mini Kit (Cat no. 12183018, Invitrogen, United Kingdom). First-strand cDNA was prepared using a Primer Script First Strand cDNA Synthesis Kit (Cat no. 6210A, TaKaRa, Otsu, Japan). Quantitative-PCR (qPCR) was performed by using a Fast Start Universal SYBR Green Master (ROX) (Cat no. 04913914001, Roche, Mannheim, Germany). The specific primers for qPCR are listed in **Supplementary Table S2**. *Cullin* and the rice *Ubiquitin* gene were chosen as references for the RT-qPCR in *S. italica* tissues and the rice transgenic lines,

respectively, according to the previous reports (Martins et al., 2016; Wang Y. et al., 2017). The data were analyzed by using an Applied Biosystems 7300 Analyzer (Applied Biosystems, Foster City, CA, United States).

Flow Cytometry

For flow cytometry, approximately 100 mg of proliferating first leaves were lacerated into 1 ml of cold nuclear isolation buffer (Lin et al., 2012) and then filtered with a 74 μm mesh. The suspension liquid was then stained with 2.5 mg ml⁻¹ of 4',6-diamidino-2-phenylindole (DAPI) for 10 min and analyzed on a MoFlo XDP cytometer (Beckman Coulter, CA, United States). For each test, 8000 nuclei were record to detect the ploidy level.

Yeast One-Hybrid Analysis

For the yeast one-hybrid analysis, the bait sequences containing adaptors and three tandem repeats of binding site sequence are listed in **Supplementary Table S3** (EBS, mEBS). The coding sequences of prey proteins were amplified with the primers listed in **Supplementary Table S3** (for *Seita.4G108100*: primer pairs “4G100”; for *Seita.1G314900*: primer pairs “1G900”). The yeast one-hybrid assay was operated by using a Matchmaker Gold Yeast one-hybrid system (Cat no. 630491, Clontech, Mountain View, CA, United States).

Transcriptome Sequencing Analysis

Yugu1 and *sistl2* plants were grown under the conditions of 16 h light and 8 h dark at 28°C for 4 weeks. The fourth extending leaves of *sistl2* and Yugu1 were harvested for total RNA extraction. The transcriptome sequencing was then performed and the cDNA libraries of *sistl2* and the WT were constructed in accordance with the Illumina sequencing manual and then sequenced on an Illumina HiSeq 2500 Genome Analyzer (Illumina, San Diego, CA, United States) with three independent biological replicates. Raw sequencing data were deposited with EMBL-EBI in the European Nucleotide Archive database under the accession number ERP106657. The qRT-PCR primers for the validation of the RNA-seq results are listed in **Supplementary Table S9**.

Carbon Isotope Determination and Low CO₂ Treatment

Approximately 50 mg of mature leaf samples at the heading stage of Yugu1 and *sistl2* were harvested. The samples were dried off at 80°C for 24 h. Pulverized samples were then disposed in accordance with a method described in a previous study (Cousins et al., 2008). The carbon isotopes were measured by using a Thermo Fisher Delta V isotope ratio mass spectrometer and calculated from a previously described equation (Stutz et al., 2014).

To verify how a low CO₂ environment impacts *SiSTL2* and photosynthesis-associated genes, 4-week-old plants of the WT and *sistl2* were grown in a CO₂ level control box. The CO₂ level was set to 40 ppm with 16 h of light and 8 h of dark at 28°C. To avoid the influence due to the daily fluctuation of the genes,

¹<https://phytozome.jgi.doe.gov/pz/portal.html>

²<https://www.ncbi.nlm.nih.gov/Structure/cdd/wrpsb.cgi>

³<http://www.rcsb.org/>

⁴http://plantregmap.cbi.pku.edu.cn/binding_site_prediction.php

samples are harvested from the same parts of the leaves at the same time in each day (10 o'clock a.m.).

RESULTS

Phenotypic Characterization of the *S. italica sistl2* Mutant

The *S. italica* stripe leaf mutant *sistl2* was isolated from EMS-induced Yugu1 cultivar. Before the three-leaf stage, the phenotype of the mutant was normal, except for the white striped first leaf (Figures 1A–D). From the fourth leaf, *sistl2* begins to display white striped leaves (Figure 1B). At the shooting and heading stage, *sistl2* exhibited decreased plant height, impaired plant development, and notable narrow leaves covered with white stripes (Figures 1E,G). However, the grain size of the mutant was not affected (Figure 1E).

Several key agronomic traits of WT and *sistl2* were also surveyed. The results proved that the entire plant development of *sistl2* was arrested (Supplementary Table S4). It is worth noting that the leaf length and leaf width were clearly reduced; in addition, the panicle size, panicle weight, and seed setting percentage in *sistl2* also decreased extensively (Figure 1H and Supplementary Table S4). These results indicated that leaf extension and reproductive development were impaired in *sistl2*.

C₄ Typical Plant Leaf Structure and Development Was Seriously Defective

To investigate the changes in the leaf anatomy structure in *sistl2*, we observed the leaves by using a portable digital microscope. The results showed that the leaf veins of WT were complete. Bundle sheath (BS, contain more and larger chloroplasts), mesophyll tissue (M, contain less and smaller chloroplasts), and vascular bundles (VBs, without any chloroplasts) array neatly (Figure 2A). In contrast, some leaf veins of *sistl2* are misshapen and array in a disordered fashion (Figure 2B, red arrows). This result can also be confirmed by the I₂–KI staining on the leaves of WT and *sistl2* (Figures 2C,D). Because of different starch accumulation in chloroplast, BS and M can be dyed different color by I₂–KI. The BS and M of WT were dyed brown and yellow, respectively, and arrayed neatly. These results showed that the leaf veins of WT were intact and regular (Figure 2C). However, some veins of *sistl2* are discontinuous (Figure 2D, red arrows).

To further assess the anatomical traits, cross sections of the leaf were obtained (Figures 2E,F). In the leaves of Yugu1, the Kranz structure is regular; mesophyll cells (MCs) and bundle sheath cells (BSCs) contain many chloroplasts which are dyed purple (Figure 2E, yellow arrows). As a typical C₄ plant, *S. italica* has a constant leaf vein distance; between the two leaf veins (V) there are always two to three MCs in WT leaves (Figure 2E). Compared with the WT, the Kranz structure of *sistl2* was irregular. Although some BSCs and MCs are normal (Figure 2F, yellow arrows), many have fewer chloroplasts or even do not contain any chloroplast (Figure 2F, red arrows). In addition, for some leaf veins of *sistl2*, the BSCs appear to be undeveloped or absent

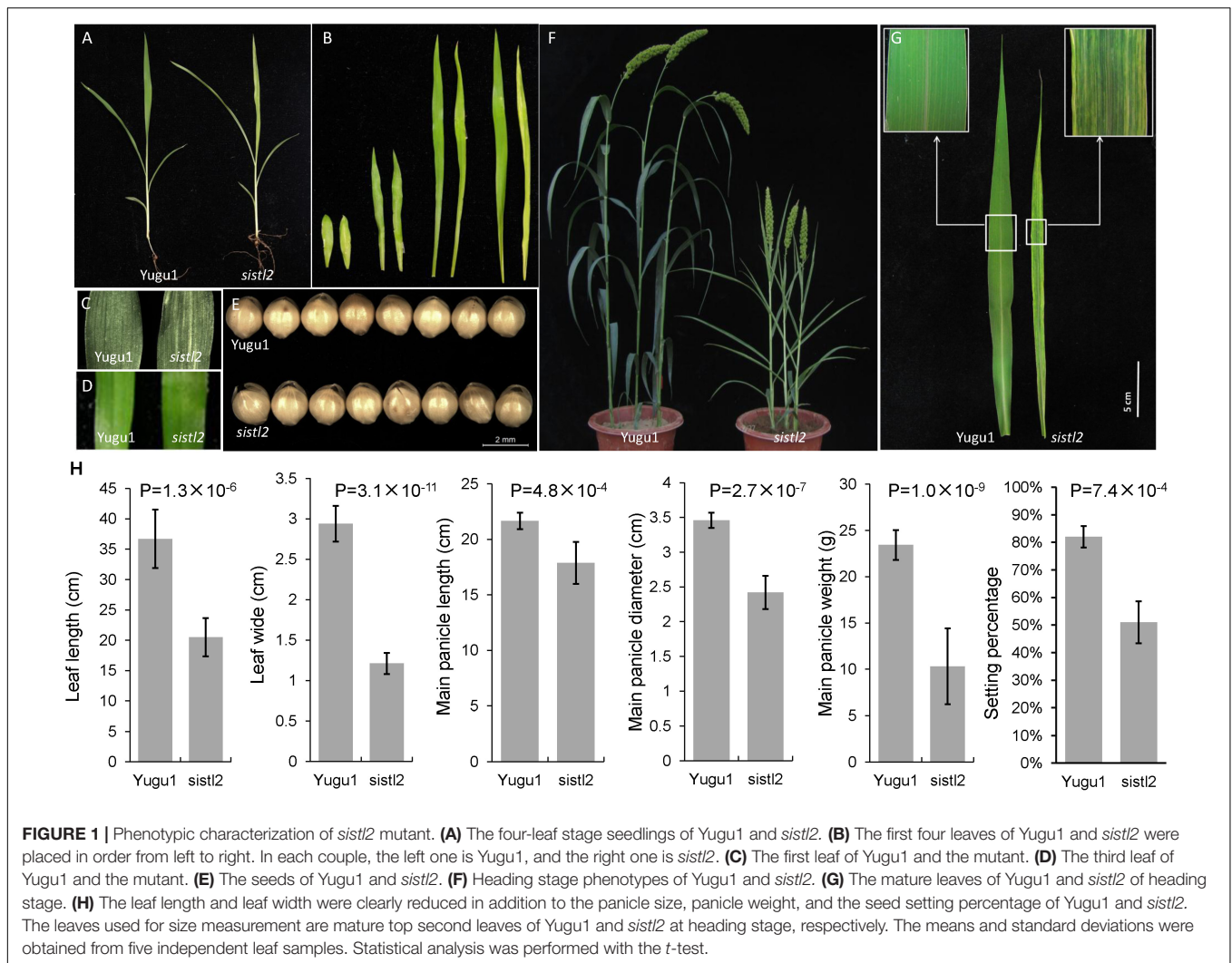
(Figure 2F, gray polygons) and there is only one MC between the two veins (Figure 2F, blue arrow). In addition, it is worth noting that the sizes of BSCs and MCs in *sistl2* were decreased to 43.52 and 40.27% of that in the WT, respectively (Figure 2G). These results indicated that the chloroplast biogenesis and the leaf cell expansion of *sistl2* were inhibited and that the leaf anatomical structure was also impaired.

To further investigate the influences on *sistl2* chloroplast biogenesis, mature leaves of *sistl2* and WT were observed by TEM, as shown in Figure 3. The Kranz structures of the WT and the *sistl2* mutants are shown in Figures 3A,B, respectively. Normal and abnormal (red arrows in Figure 3B, these cells have less or no chloroplast) BSCs/MCs could be observed in *sistl2*. The chloroplasts in the normal MCs of *sistl2* were similar to the WT, containing fully developed stroma lamellas and granum lamellas (Figures 3E,F). As *S. italica* is an NADP-ME type C₄ plant, the BSCs contain only stroma lamellas. The chloroplasts in normal BSCs of *sistl2* also have well-developed stroma lamellas (Figures 3C,D). However, some BSC chloroplasts of *sistl2* contained fewer starch grains relative to the number found in Yugu1 (Figures 3C,D). In contrast, the chloroplasts in the abnormal BSCs/MCs of *sistl2* seem to be undeveloped (Figures 3G,H; red arrows). These results further clarify that the formation of Kranz structure, the leaf cell development, and chloroplast biogenesis in *sistl2* were significantly impaired.

Genetic Mapping of the *SiSTL2* Locus and Bioinformatics Analysis

Fine mapping was performed by the means of MutMap+ by using the M₄ population (Fekih et al., 2013). The *SiSTL2* locus was mapped to a 12 Mb genomic region from 46.8 to 58.9 Mb on chromosome 9 (Figure 4A, gray box). In accordance with the requirement for the index of homozygous recessive mutation should be greater than 0.9, four putative mutation sites were identified (Supplementary Table S5). In addition, an F₂ mapping population was generated from a cross between *sistl2* with the SSR41 cultivar. Through the use of this F₂ population (120 individuals with striped leaves), a 1 Mb genomic region between the In-Del marker Ins9-1 and the SSR marker b171 was defined (Figure 4A). Among those four putative mutations, only the mutant site of a G to A mutation at 54,317,059 on chromosome 9 is included in this region and it is predicted to lead a splice site alteration at *Setaria.9G511200*. *Setaria.9G511200* was assumed to have nine exons and eight introns, with the G to A mutation located at the last base of the third intron. The transcript sequence verified that this mutation caused the first base of the fourth exon to be altered to the last base of the upstream intron, which further leads to a single-base deletion of the coding sequence (Figure 4B) and resulted in a frame shift and a premature stop codon at the fifth exon.

Gene annotation revealed that *SiSTL2* encoded a putative *Setaria* deoxycytidylate (dCMP) deaminase. *SiSTL2* encoded a 228 amino acid peptide chain. The protein structure domain, as predicted by NCBI, showed that *SiSTL2* comprised a dCMP deaminase (DCD) domain from amino acids 71 to 184. Six catalytic motifs and four Zn²⁺ binding sites were located in this domain, which were essential for catalytic function. However, the



mutation occurred at amino acid 107. As a result, the mutant SiSTL2 protein (Δ SiSTL2) lacks all the functional motifs and a large section of the DCD domain, which caused a defective protein function (Figure 4C). The SiSTL2 3D protein structure of the WT and *sist2* were modeled (Figure 4D). These results showed that the SiSTL2 protein contained five alpha helices and eight beta sheets, which functioned as a homo-hexamer, which forms a hexagon. However, Δ SiSTL2 loses four alpha helices and six beta sheets, so that it cannot form any homo-multimer (Figure 4D).

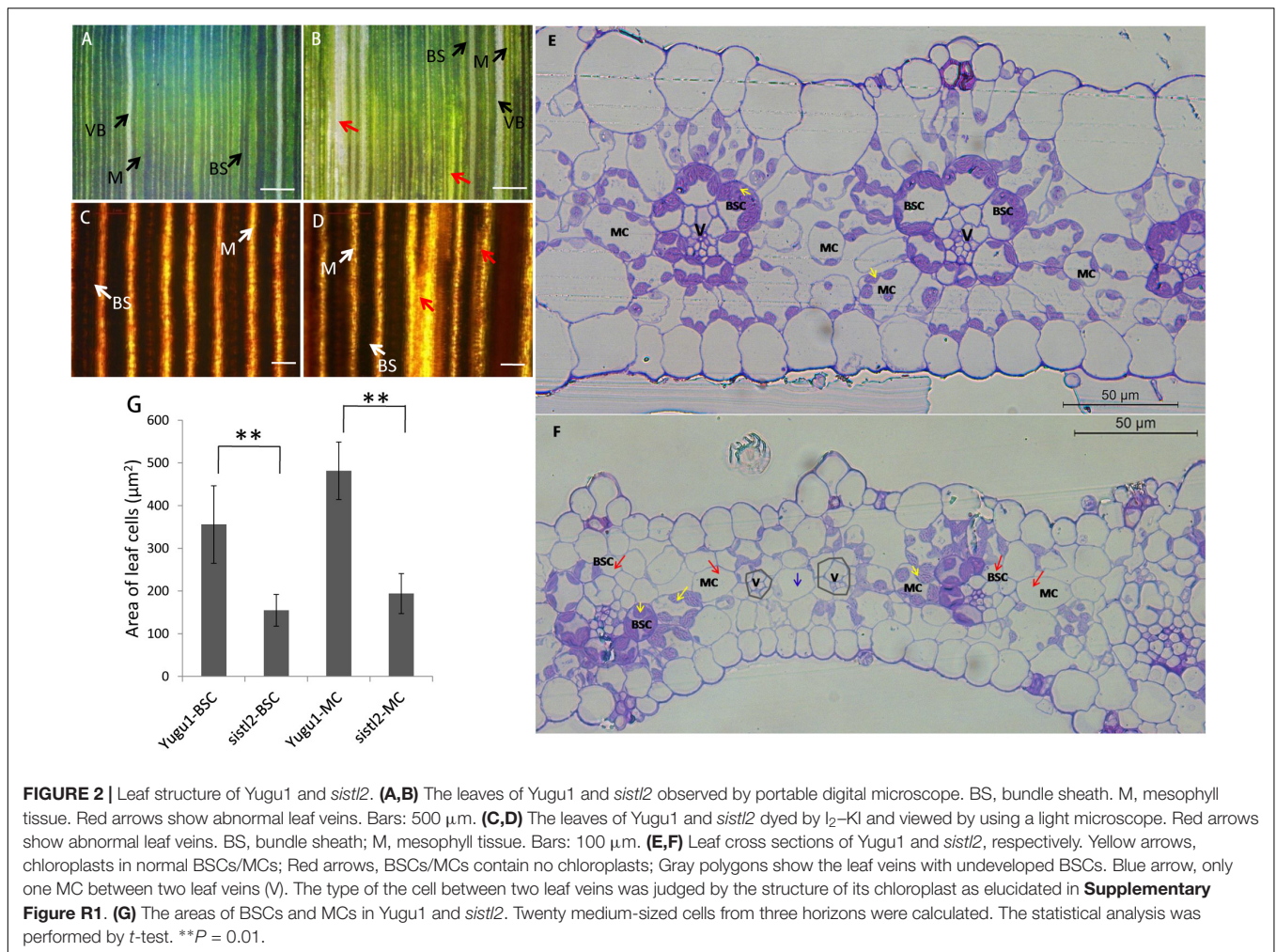
SiSTL2 Can Complete the Phenotype of the *OsDCD* Mutant

The protein sequence BLAST showed that SiSTL2 was a homologous protein of *Oryza sativa* OsDCD. Owing to the difficulty of *S. italica* transformation, we choose the *OsDCD* mutant *st2*, which has a similar phenotype to *sist2*, to perform the complementation assay. A fragment harboring a 6.75 kb genome sequence of *Setaria*.9G511200, which contains a promoter and a 3'-UTR is introduced into *st2*. All five positive

transgenic lines exhibited normal phenotypes. The phenotype and chlorophyll content of complemented T_0 (Com) was restored to WT (Figures 5A,B). The transcript of *SiSTL2* accumulated abundantly in transgenic lines, but did not exist in *st2* and the WT (Figure 5C). These results indicated that SiSTL2 had a similar function to OsDCD and was responsible for the stripe-leaf phenotype.

DCD Deamination Activity and Chloroplast Development Are Impaired in *sist2*

To gain whether SiSTL2, the homolog of OsDCD, has DCD deamination activity, wild-type SiSTL2 protein with histidine tag (His-SiSTL2) and mutant SiSTL2 protein with histidine tag (His- Δ SiSTL2) were purified (Supplementary Figure S1). Then an *in vitro* assay was performed to test the deamination activity of SiSTL2 and Δ SiSTL2 (Figure 6A). The kinetic assay showed that with the substrate concentration increased, the deamination activity of the recombinant His-SiSTL2 rose and reached maximum. However, His- Δ SiSTL2 almost has no



deamination activity (**Figure 6A** and **Supplementary Figure S1**, histidine tag protein as a negative control). This result indicate that SiSTL2 has deamination activity and can catalyze the deamination of dCMP. However, when the C terminal of the protein is deleted, Δ SiSTL2 lost the deamination activity.

To study the influence on transcription level caused by the mutation of *SiSTL2*, the relative expression levels of *SiSTL2* were verified in leaves at the seedling stage (**Figure 6C**). The results showed that the transcription levels of *SiSTL2* in the mutant was significantly reduced compared with Yugu1. This result indicated genes involved in *de novo* pathway and the salvage pathway of dTTP biosynthesis were affected. As the pyrimidine triphosphate salvage pathway is also essential for dTTP synthesis, the relative expression levels of several salvage pathway genes (*SiTK1*, *SiUDK*, *SiUDN*, and *SiCDA*) were also determined (**Figures 6B,C**). The results showed that the expression of salvage pathway genes in the mutant was also decreased. These results suggested that the mutation in *SiSTL2* influenced both the *de novo* pathway and the salvage pathway of dTTP biosynthesis.

To explain the white stripe formation in *sistl2*, the expression levels of chloroplast development associated genes were also

detected. The results indicated that the transcription levels of most of these genes were significantly lower in *sistl2* (**Figure 6D**), which suggested that the chloroplast development was impaired at the transcriptome level. However, whether this transcription decline is result from the dTTP biosynthesis is still unclear.

***SiSTL2* May Be Controlled by E2F and Is Involved in Cell Cycle Regulation**

Deoxycytidine monophosphate deaminase decreases can sometimes impair the mitosis cell cycle progression (Niu et al., 2017). Thus, the DNA ploidy levels of leaf cells in the WT and *sistl2* were determined by using flow cytometric analysis. The first leaves of Yugu1 and *sistl2* were harvested at 48 h after germination sprout. The results displayed that *sistl2* has higher percentage of 2C cells, but less 4C and 8C cells than Yugu1 (**Figures 7A,B**). In other words, in *sistl2*, more cells were present in the G1/S-phase and fewer cells were in the G2/M-phase than those in the WT. This result indicated that the mitotic cell cycle of *sistl2* was delayed at the transition from the G1/S- to the G2/M- phase.

It has been reported that the expressions of DCD and many other nucleotide biosynthetic genes were coordinated with cell

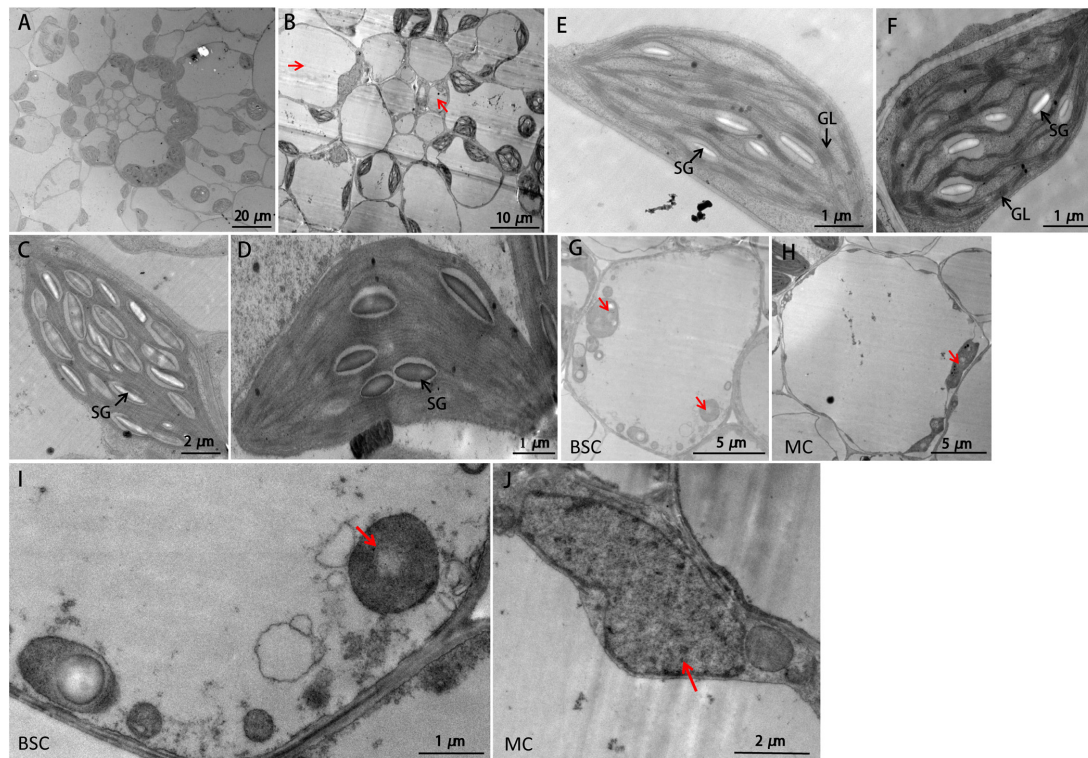


FIGURE 3 | TEM images of WT and *sistl2*. **(A,B)** Kranz structures of Yugu1 and *sistl2*, respectively. Red arrows, abnormal BSCs and MCs. **(C,E)** The chloroplasts in BSC and MC of Yugu1, respectively. The structure of an individual BSC chloroplast (WT) was shown in **Supplementary Figure R2**. **(D,F)** The chloroplasts in normal BSC and MC of *sistl2*, respectively. SG, starch granules; GL, grana lamella. Abnormal BSC **(G)** and MC **(H)** in *sistl2*. Red arrows show the undeveloped chloroplasts. **(I,J)** Undeveloped chloroplast in BSC and MC.

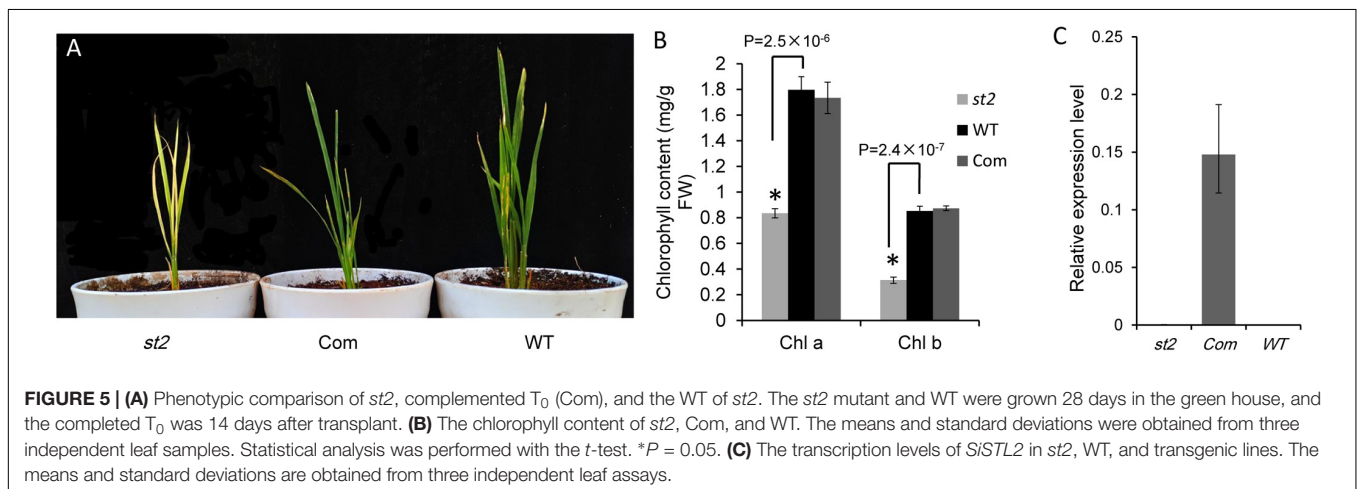
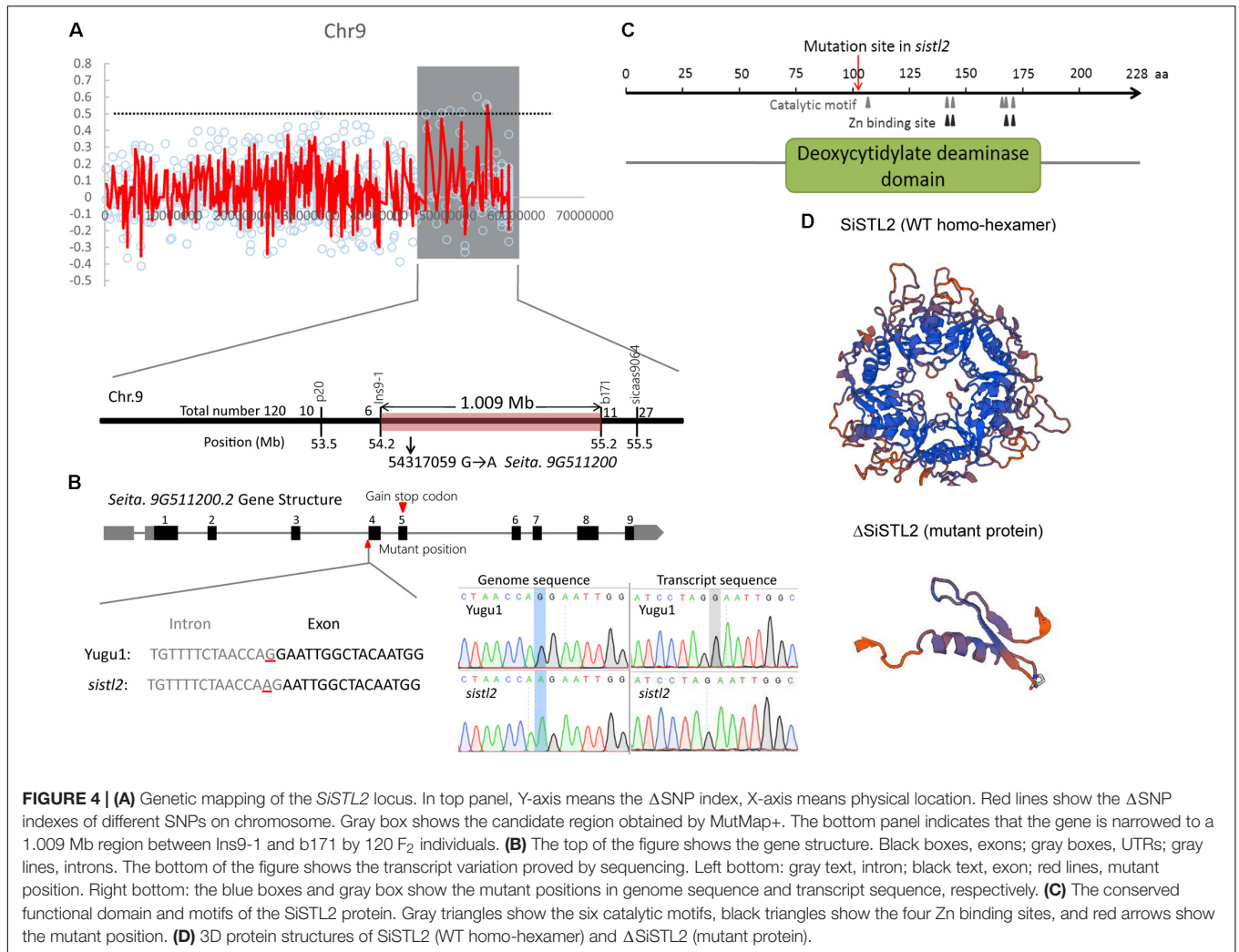
cycle progression and regulated by some cell cycle-associated enzymes (Ke et al., 2005). We also considered whether the expression of *SiSTL2* was controlled by any cell cycle-related proteins. Thus, the *cis*-acting elements in the *SiSTL2* promoter were predicted and an E2F transcription factor binding site (EBS) (CCCCAAAGTTTCCCGCGCTTA) was found at -99 to -119 bp upstream of the initiation codon of *SiSTL2*. A random sequence (mEBS) (TCGCATCTGCCACCTCAGTAC) of the same length as EBS was considered to represent a negative control. Then, we verified the interactions between the EBS element and the SiE2F proteins by using the yeast one-hybrid assay (**Figure 7C**). The results showed that *Seita.4G108100* and *Seita.1G314900*, which are homologs of E2F ϵ , could bind to the EBS of the *SiSTL2* promoter and activate the expression of the *Aureobasidin A* (AbA) resistance gene in yeast strains. E2F family members are TFs that are closely related to the regulation of cell cycle progression. Collectively, these results suggested that *SiSTL2* may be regulated by cell cycle-related E2F ϵ and impacted cell cycle progression. Defective *SiSTL2* resulted in blockage of the cell cycle.

Comparison of Genome-Wide Transcriptomes of WT and *sistl2*

Deoxycytidine monophosphate deaminase is a key enzyme in the regulation of the synthesis of dTTP. The lack of dTTP

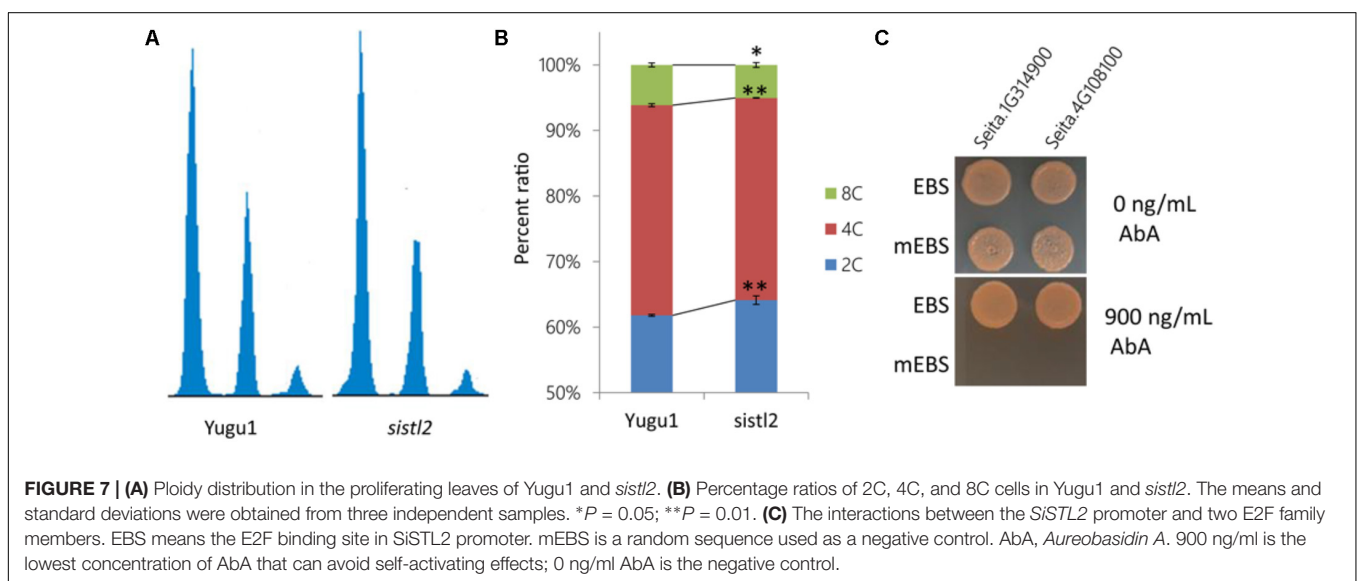
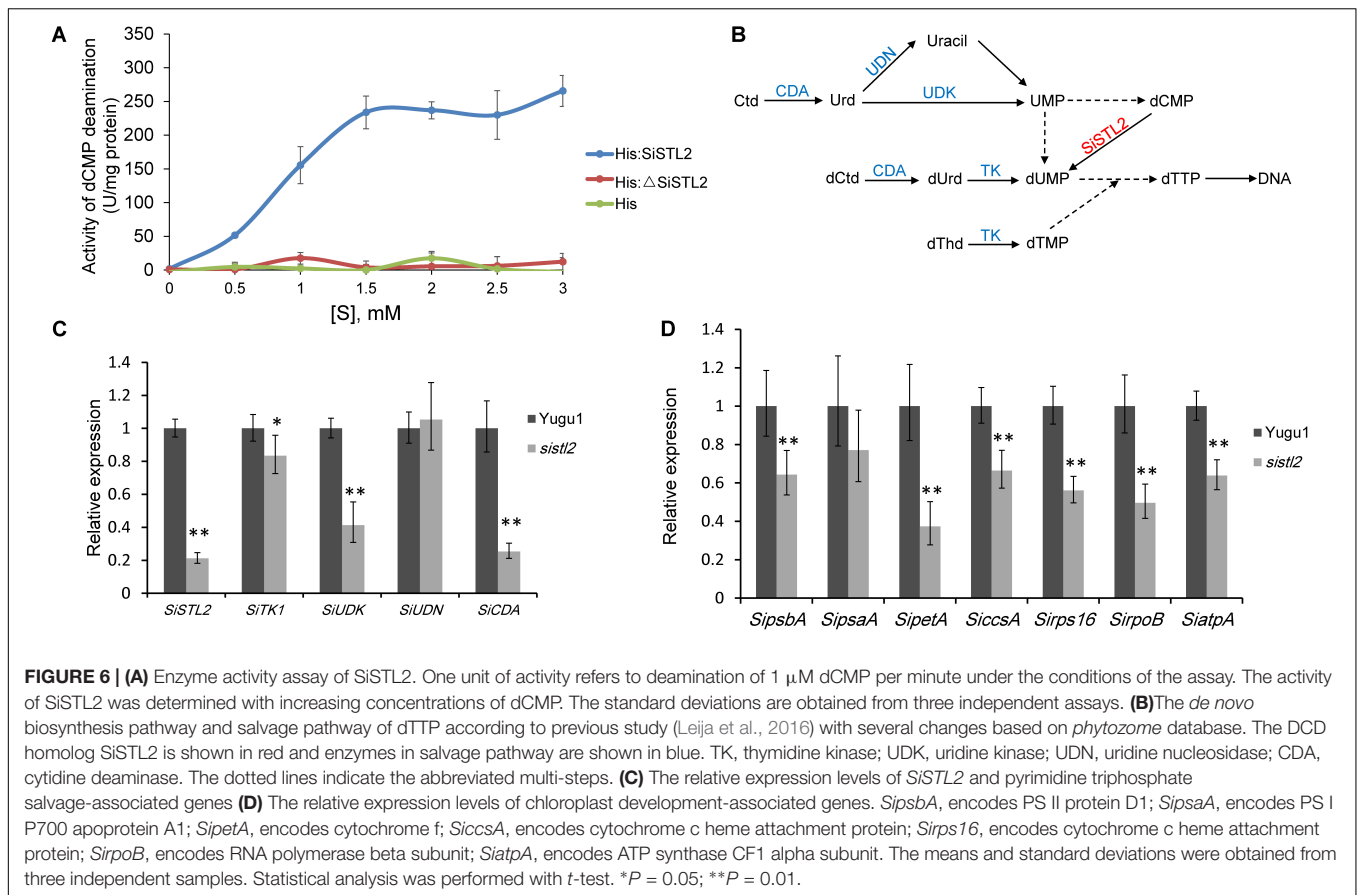
may impact DNA replication and further influence the other aspects of growth and development. The *sistl2* mutant showed comprehensive abnormal phenotypes of plant height, panicle size, seed-set rate, and especially leaf development. Thus, to reveal the signaling pathways and the regulatory networks that changed in the *sistl2* mutant, and to explain the relationships between *SiSTL2* and leaf or chloroplast development, the genome-wide transcriptomes of leaves of Yugu1 and *sistl2* were compared. The fourth leaves during extension were chosen as the material for RNA sequencing.

The analysis detected 2694 different expressed genes (DEGs) between Yugu1 and *sistl2* (**Supplementary Table S6**). The enriched KEGG pathways of the top 10 DEGs are listed in **Table 1**. The data showed that the DEGs were most concentrated in photosynthesis associated pathways (photosynthesis, carbon fixation in photosynthetic organisms, and photosynthesis-antenna proteins) and DNA replication associated pathways (DNA replication and mismatch repair). Genes associated with carbon metabolism and secondary metabolite (fatty, glyoxylate, and phenylpropanoid) biosynthesis and metabolic pathways were also extensively changed. The results of Gene Ontology (GO) analysis showed that DEGs were enriched in GO terms related to photosynthesis, cell cycle progression, DNA replication, and microtubule (involved in spindle formation) (**Figure 8A**).



Given the function of *SiSTL2* and the phenotypes of the *sistl2* mutant, we selected DEGs in the pathways associated with photosynthesis, DNA replication, chlorophyll metabolism, hormone signals, and carbon metabolism and analyzed the

changes in expression (**Figure 8B** and **Supplementary Table S7**). Most of the DEGs in photosynthesis-associated pathways and chlorophyll metabolism were down-regulated, which was consistent with the decreased capacity of photosynthesis and



chlorophyll content of *sistl2*. Almost all of the DEGs in nucleotide metabolism, DNA replication and mismatch repair pathways were up-regulated; this may be caused by feedback regulation of the SiSTL2 functional defect. DEGs in carbon metabolism and glyoxylate/dicarboxylate metabolism generally were down-regulated, indicating that energy conversion may

be impaired in *sistl2*. DEGs in hormone signal pathways showed great changes, especially several auxin and cytokinin response regulator genes were sharply up-regulated (*SiIAA26*, 1.80 fold; *SiLAX2*, 1.74 fold; *SiARR12*, 2.14 fold; *SiARF5*, 2.31 fold; *SiDFL1*, 5.50 fold; *SiARR9*, 1.99 fold; *SiTGA9*, 2.58 fold). This suggested that hormone regulators that

promote growth respond positively to the development of plant retardation. Most DEGs that participate in cell cycle regulation were up-regulated, which was consistent with the results of flow cytometric analysis and the yeast one-hybrid assay.

The expression changes of some associated TFs are summarized in **Figure 8C** and **Supplementary Table S8**. It is noteworthy that some TFs families are generally up-regulated, such as Teosinte Branched 1/Cycloidea/Proliferating Cell Factor (TCP), E2F, Growth Regulating Factor (GRF), YABBY, and Auxin Response Factor (ARF). Among these TFs families, ARF, E2F, and GRF control the leaf growth and development by regulating cell proliferation (Kim et al., 2003; Horiguchi et al., 2005, 2006; Magyar et al., 2005; Guilfoyle and Hagen, 2007; Lim et al., 2010). TCP family members are responsible for the progress of leaf expansion and development (Martin-Trillo and Cubas, 2010; Efroni et al., 2013). YABBY can regulate the leaf axial development (Sarojam et al., 2010). Additionally, some members of ARF and GRF are speculated to be associated with C₄ photosynthesis in maize (Wang et al., 2013; Ding et al., 2015). However, some other TFs families also may be associated with leaf patterning, plastid biogenesis, and photomorphogenesis, such as MYB, GLK, bHLH, GRAS, and GATA (Wang et al., 2013). These TFs are also speculated to participate in C₄ photosynthesis (Wang et al., 2013; Wang P. et al., 2017). Members of these TFs families are numerous. In *sistl2* mutant, many members of these TFs up-regulated or down-regulated sharply compared with that in WT. This indicates that the expression of these TFs are influenced in the mutant (**Figure 8C**). Collectively, the leaf development and C₄ photosynthesis may be impaired because of the mutation of *SiSTL2*. In addition, to validate the RNA-seq, 13 genes were selected and detected by qRT-PCR (**Supplementary Figure S2**). These genes are associated with photosynthesis, DNA replication, and cell cycle, encoding PS I/II reaction center proteins (Seita.J018400, Seita.3G149000, Seita.3G184900, and Seita.6G032200), chlorophyll binding protein (Seita.6G158500), DNA polymerase subunits (Seita.6G050100 and Seita.5G394500), DNA replication licensing factor (Seita.1G352100), cycle division control proteins (Seita.4G045900 and Seita.2G283000), and cyclins (Seita.9G171000, Seita.5G005800, and Seita.5G352700). The consequences are correspond to that in RNA-seq.

***SiSTL2* Affects C₄ Photosynthesis Capacity in Foxtail Millet**

To investigate the influence of *SiSTL2* on the capacity for C₄ photosynthesis, the photosynthetic index, chlorophyll fluorescence kinetic parameters, and chlorophyll (Chl) accumulation were detected in *sistl2*. The results showed that compared with Yugu1, the net photosynthetic rate of *sistl2* was decreased by 46.1%; the stomata conductance was decreased by 45.6%; the transpiration rate declined by 65.2%, whereas the intercellular CO₂ concentration showed no significant difference compared with that in Yugu1, concurrently. This suggested that the photosynthetic capacity of *sistl2* was impaired,

which led to the accumulation of intercellular CO₂. The Φ PSII reflects the light absorbed by PS II that is used in photochemical reactions. Fv'/Fm' indicates the excitation energy capture efficiency, which is also reflective of the light portion used in photochemistry. The significant decrease in these two indices of *sistl2* indicated that light-use efficiency was influenced by the mutation (**Figure 9A**). Interestingly, Chl *a* content was not influenced, whereas the Chl *b* content and total Chl content was significantly decrease in the *sistl2* mutant (by approximately 67 and 18%, respectively; **Figure 9B**). It has been reported that the degradation of Chl *b* is prior to Chl *a*, and can translate to Chl *a* (Schelbert et al., 2009). This is consist with our result.

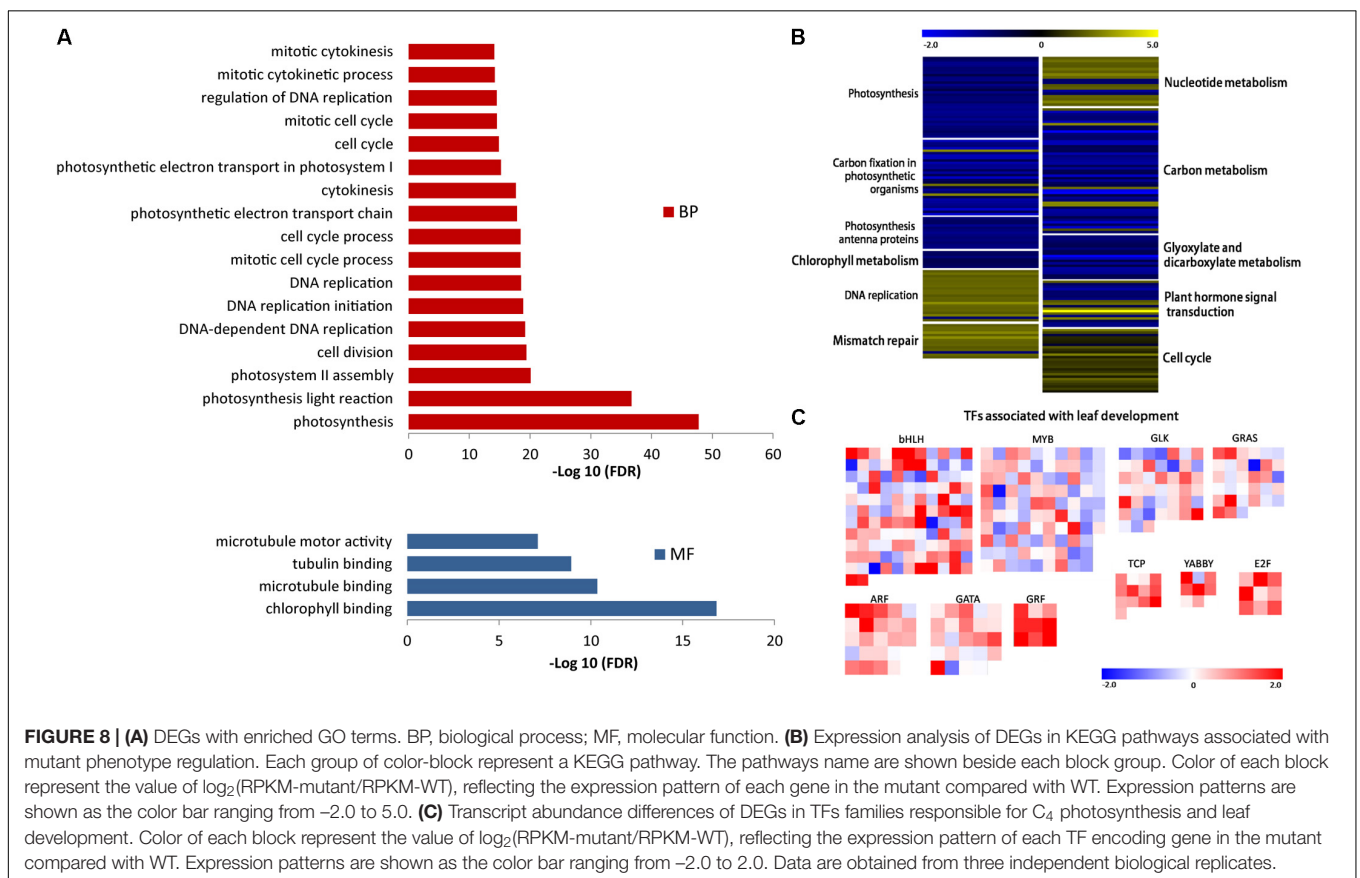
As described in **Figure 3B**, the leaf Kranz structure of the *sistl2* mutant is defective. The results of RNA-seq also suggested that the C₄ photosynthesis of *sistl2* may be affected. To confirm this, the stable carbon isotopes of the *sistl2* mutant, Yugu1, and a rice *Japonica cultivar*, as a C₃ control, were measured. The atmosphere contains a small amount of ¹³C. When C₃ plants fix CO₂, Rubisco prefers ¹²CO₂. However, the C₄ photosynthetic CO₂ fixation enzyme PEPC does not tend to function on ¹²CO₂. Rubisco of C₄ plants only exists in BSCs which segregates rubisco from air. As a result, ¹³C accumulates to a greater extent in C₄ plants than in C₃ plants. It has been reported that C₃ plants and C₄ plants can be identified by the value of $\Delta^{13}\text{C} \text{‰}$ (C₃: -32 to -23‰; C₄: -19 to -6‰) (Bender, 1971). Our data show that $\Delta^{13}\text{C} \text{‰}$ in *sistl2* was significantly decreased by 4.87% (**Figure 9C**), although the value was still within the range of C₄. Then, we tested the expression of *SiSTL2* and certain C₄ photosynthesis-related genes that respond to the stress of low CO₂ environments. The results showed that in Yugu1, the expression level of *SiSTL2* was rapidly up-regulated until 12 h, decreased to the initial level, and remained stable. However, in *sistl2*, the transcription level remained at a low level until 24 h and started to increase after 36 h (**Figure 9D**). This suggested that the expression of *SiSTL2* can respond in a timely manner to the low CO₂ level. The mutation in *SiSTL2* resulted in a delayed response to the stress of a low CO₂ environment. The C₄ photosynthesis-related genes (Ding et al., 2015; Huang et al., 2017) showed a similar expression pattern to *SiSTL2* in low CO₂ conditions, which increased to a peak value at 12 h and then returned to the initial level (**Figure 9E**). In conclusion, we speculated that *SiSTL2* might indirectly regulated C₄ photosynthesis.

To further verify the connection between *SiSTL2* and C₄ photosynthesis, transcript levels of 102 previously reported *S. italica* C₄ candidate genes (Ding et al., 2015) in WT and *sistl2* are summarized from our RNA-seq data (**Supplementary Table S10**). According to the expression patterns differences between C₃ and C₄ species, these genes are divided into three types. Type I including genes that have higher expression levels in C₄ leaves compared with C₃ leaves. Type II genes show different expression patterns between C₄ and C₃ species. Type III genes have orthologs in C₄ species but absent in C₃ species (Ding et al., 2015). Comparison result showed that most of these genes (89 of 102; Type I, 18 of 20; Type II, 59 of 65; Type III, 12 of 17) also changed their

TABLE 1 | DEGs most enriched KEGG pathways.

Pathway	DEGs with pathway annotation (454)	All genes with pathway annotation (5291)	P-value	Q-value	Pathway ID
Photosynthesis	33 (7.27%)	82 (1.54%)	2.97×10^{-15}	3.09×10^{-13}	ko00195
Carbon fixation in photosynthetic organisms	31 (6.83%)	83 (1.56%)	2.40×10^{-13}	1.25×10^{-11}	ko00710
Photosynthesis – antenna proteins	13 (2.86%)	16 (0.3%)	4.69×10^{-12}	1.63×10^{-10}	ko00196
DNA replication	21 (4.63%)	67 (1.27%)	7.04×10^{-8}	1.83×10^{-6}	ko03030
Carbon metabolism	51 (11.23%)	293 (5.5%)	3.70×10^{-7}	0.000007	ko01200
Fatty acid elongation	15 (3.3%)	48 (0.91%)	5.64×10^{-6}	0.000106	ko00062
Mismatch repair	14 (3.08%)	49 (0.93%)	0.000039	0.000581	ko03430
Glyoxylate and dicarboxylate metabolism	18 (3.96%)	77 (1.46%)	0.000063	0.000815	ko00630
Phenylpropanoid biosynthesis	41 (9.03%)	264 (4.99%)	0.000106	0.001226	ko00940
Phenylalanine metabolism	12 (2.64%)	50 (0.95%)	0.000815	0.008471	ko00360

The English in this document has been checked and edited by two professional editors, both native speakers of English. For a certificate, please see the upload file "Certificate_of_editing-SRATA_1.pdf."



expression patterns in *sistl2* mutant (Supplementary Table S10). Moreover, expression of 25.5% of these genes decreased more than twofolds in *sistl2* compared with WT. According to the previous study (Ding et al., 2015), C_4 candidate genes which are associated with C_4 photosynthesis in leaves and C_4 evolution are also summarized, respectively (Supplementary Figure S3, right panel and Supplementary Table S10). The result showed that 87.8% C_4 photosynthesis associated genes (43 of 49) and 86.0% C_4 evolution associated genes (37 of 43) are down-regulated in *sistl2*. These results further

indicated that the mutant in *SiSTL2* has some linkage with C_4 photosynthesis.

DISCUSSION

Comparison of DCD Mutant Characteristics in Foxtail Millet and Rice

In *sistl2*, the plant height and chlorophyll contents were significantly decreased, the leaves have white stripes (Figure 1).

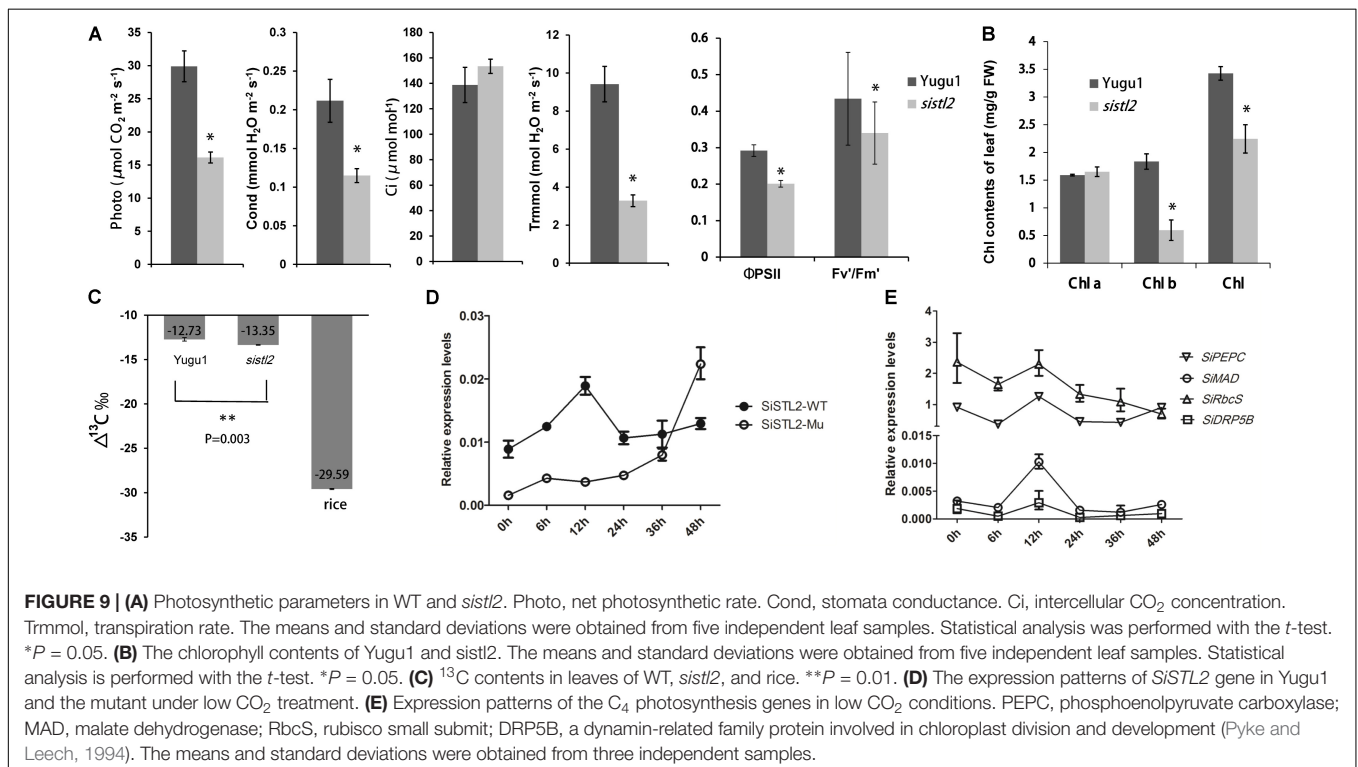
Furthermore, some leaf cells in *sistl2* contain fewer chloroplasts or even have no chloroplast (Figures 2E,F). All these phenotypes were quite similar to the mutants of *OsDCD* (Xu et al., 2014; Niu et al., 2017). This suggested that the function of SiSTL2 is similar to that of *OsDCD*. What's more, similar phenotypes also exist in the mutants of other dNTP synthesis associated genes and other species (Yoo et al., 2009; Qin et al., 2017). Thus we speculate that there are some correlations between dNTPs synthesis and leaf/chloroplast development, which need more experiments and evidences to prove it. In our study, the cell cycle progression of *sistl2* was impaired (Figures 7A,B), DEGs were enriched in the cell cycle GO term (Figure 8A) and most of the cell cycle-associated genes were up-regulated (Figure 8B). In the *alr* mutant, the cell cycle progression was also delayed (Niu et al., 2017). This indicated that SiSTL2 played a similar role in cell cycle regulation to *OsDCD*. In addition, the dNTP pools in *alr* were unbalanced. This caused further defects in DNA replication and repair (Niu et al., 2017). Our results show that SiSTL2 also has deamination activity similar with *OsDCD* (Figure 6A). In *sistl2*, the results of RNA-seq showed that abundant DEGs were enriched in the DNA replication and mismatch repair pathways (Table 1). In addition, most DEGs associated with nucleotide metabolism, DNA replication, and mismatch repair were up-regulated, which may be caused by feedback control (Figure 8B). These results suggested that similar to *OsDCD*, SiSTL2 can regulate DNA replication and repair. In addition, the expression levels of chloroplast development-associated genes in *sistl2* were significantly decreased relative to Yugu1 (Figure 6C). The same results were also obtained in *alr*

mutant (Niu et al., 2017), indicating that SiSTL2 disruption can impair chloroplast development. In summary, SiSTL2 has a similar function to *OsDCD*, and has effects on DNA replication and repair, cell cycle progression, and chloroplast development.

SiSTL2 Participates in the Regulation of Cell Division and Influences Cell Expansion

The leaves of the *sistl2* mutant were significantly smaller than that of Yugu1 (Figure 1H and Supplementary Table S4). The smaller sizes of organs usually from a reduction in cell number or cell size. These two parameters always depend on cell proliferation and cell expansion.

In our study, the ratios of 4C and 8C cells are significantly lower in *sistl2* compared with the level in Yugu1 (Figures 7A,B). We also found that in the vasculature of *sistl2*, the number of MCs and BSCs was reduced (Figure 2F). This indicated that the cell cycle progression in *sistl2* was delayed and that the cell proliferation may be defective. RNA-seq also showed that cell cycle-related genes (Figure 8A) and TFs (E2F; Heuvel and Dyson, 2008) suggesting that cell cycle of *sistl2* is influenced. Some reports indicated that many dNTP synthesis-associated genes were controlled by cell cycle regulating proteins (Ke et al., 2005). RNR, as an upstream gene of DCD and the S-phase check point, can active the cell cycle going into S-phase under the control of cell cycle regulating transcription factor E2F5 (Lincker et al., 2004). The promoter of SiSTL2 also has binding sites of SiE2Fe (Figure 7C). Thus, we speculated that SiSTL2, similar to RNR,



maybe be correlated with cell cycle regulation. However, SiE2F5 is predicted to have the opposite function relative to E2F5 in cell cycle regulation. Therefore, the role of SiSTL2 in the cell cycle required further exploration.

However, the leaf cell sizes of both BSCs and MCs in *sistl2* were also significantly decreased (Figures 2F,G), which indicated that the cell expansion of *sistl2* was also impacted. The RNA-seq data showed that TFs associated with cell expansion, such as TCP and GRF (Kim et al., 2003; Martin-Trillo and Cubas, 2010), were up-regulated. This suggested that the mutation in SiSTL2 also impaired cell expansion. In addition, *sistl2* the decreases in cell sizes (by 43.52% in BSCs and 40.27% in MCs) were as strong as those in leaf length (44.1% reduction) and leaf width (58.8% reduction) relative to Yugu1 (Figure 2G and Supplementary Table S4). However, the cell cycle progression changes were not so strong (Figure 7B). Therefore, we surmised that SiSTL2 may participate in cell cycle regulation and influence the cell expansion. In *sistl2*, the smaller leaf size was mainly caused by defective cell expansion, with reduced cell proliferation a subordinate reason for the smaller leaf size.

SiSTL2 May Have an Impact on C₄ Photosynthesis

Chloroplast development is important for photosynthesis, and the Kranz leaf structure is a characteristic and precondition of C₄ photosynthesis. In *sistl2*, some BSCs and MCs have fewer or even no chloroplasts (Figures 2E,F) and the expression of chloroplast development genes are also decreased (Figure 6D). This suggested that the mutation in SiSTL2 may affect the chloroplast development at transcription level. Considering that the chloroplast genes transcription depend on both nucleus-encoded RNA polymerase and plastid-encoded RNA polymerase, we speculate that the defect of SiSTL2 may have some influence on the nucleus or plastid transcription system. Additionally, *sistl2* displayed some abnormal phenotypes with respect to Kranz structure, such as undeveloped veins, reduced BSCs and decreased mesophyll cell number between vascular bundles (Figures 2E,F). This may be the result of the restraints in both cell expansion and cell division. However, many members of the TFs families that regulate leaf development and leaf cell differentiation, such as YABBY, bHLH, GRAS, and GATA (Siegfried et al., 1999; Wang et al., 2013) are differently expressed in *sistl2*. These suggested that mutations in SiSTL2 influenced the leaf development and leaf structure. Meanwhile, most genes in the carbon fixation pathways in photosynthetic organisms were down-regulated (Figure 8A); the expression of TFs may regulate C₄ photosynthesis (ARF, MYB, and GLK) (Ding et al., 2015) changed extensively (Figure 8B). And most of the C₄ candidate genes were down-regulated after SiSTL2 was defected (Supplementary Figure S3). These suggest that there are some linkage between C₄ photosynthesis and the mutation of SiSTL2. The ¹³C accumulation in *sistl2* was also significantly reduced (Figure 9C). This suggested that the C₄ photosynthesis of the mutant was affected. Moreover, under the stress of a low CO₂ environment, SiSTL2 can

respond to the up-regulation in the similar pattern compared with C₄ photosynthesis genes (Figures 9D,E). Given that the regulation of dTTP synthesis by DCD is a relatively upstream biological pathway, we speculate that the effect of the SiSTL2 mutation is global in plants, indirectly regulating the chloroplast development and C₄ photosynthesis. As the decrease in chloroplast biogenesis, the abilities of both photosynthesis and carbon fixation were impaired seriously. In the conditions of low CO₂, the mobilization of C₄ photosynthesis genes requires sufficient dNTPs to ensure that the expression levels of SiSTL2 and C₄ photosynthesis genes are subsequently altered.

AUTHOR CONTRIBUTIONS

XD conceived the project. SZ and ST performed the data analysis and wrote the manuscript. SZ, CT, and ML conducted the experimental work. HZ provided the materials and performed the field trials. XD, ST, and GJ guided the experimental work. All authors read and approved the final manuscript.

FUNDING

This work was supported by the Fundamental Research Funds of CAAS (CAAS-XTCX2016002), the China Agricultural Research System (CARS06-13.5-A04), the National Natural Science Foundation of China (31501324), and the Agricultural Science and Technology Innovation Program of the Chinese Academy of Agricultural Sciences.

ACKNOWLEDGMENTS

We thank Zuhua He Ph.D., from the Institute of Plant Physiology and Ecology, SIBS, CAS, for providing the *OsDCD* mutant *st2*. We also thank Mei Niu Ph.D., from the Institute of Crop Science, CAAS, and Yihua Wang Ph.D., from the State Key Laboratory of Crop Genetics and Germplasm Enhancement, Nanjing Agricultural University, for providing technical guidance.

SUPPLEMENTARY MATERIAL

The Supplementary Material for this article can be found online at: <https://www.frontiersin.org/articles/10.3389/fpls.2018.01103/full#supplementary-material>

FIGURE S1 | Western blot of recombinant proteins His-SiSTL2, His-ΔSiSTL2 and His tag expressed in *E. coli*. Marker shows molecular mass in kilodaltons.

FIGURE S2 | The transcript levels of genes for validation of RNA-seq result.

FIGURE S3 | The expression analysis of the genes associated with C₄ photosynthesis in leaves and C₄ evolution. Color of each block represent the value of log₂(RPKM-mutant/RPKM-WT), reflecting the expression pattern of each gene in the mutant compared with WT. Expression patterns are shown as the color bar ranging from -2.0 to 2.0.

TABLE S1 | SSR and In-Del markers for fine mapping.

TABLE S2 | Primers used for qRT-PCR.

TABLE S3 | Primers used for yeast one-hybrid.

TABLE S4 | Characterization of agronomic traits of *sist1/2* mutant.

TABLE S5 | Putative mutation sites information.

TABLE S6 | Genes that were differentially expressed in *sist1/2* compared with the wild-type.

TABLE S7 | DEGs in mutant phenotype-associated pathways.

TABLE S8 | DEGs in phenotype-associated TFs families.

TABLE S9 | The qRT-PCR primers for the validation of RNA-seq result.

TABLE S10 | Transcript levels of C₄ candidate genes.

FIGURE R1 | Top panel, the red cycles show two leaf veins of *sist1/2*, the red box shows the cell between two leaf veins. The bottom panel shows the chloroplast (red arrow) of the cell in the red box in the top panel. The granum lamellas can be observed clearly in the chloroplast.

FIGURE R2 | (A) Kranz structure of Yugu1, the *S. italica* wild type. A chloroplast of BSC was pointed out by a blue cycle and magnified in (B). (B) The red arrows show the structures like grana in BSC chloroplast.

REFERENCES

- Bender, M. M. (1971). Variations in the 13C/12C ratios of plants in relation to the pathway of photosynthetic carbon dioxide fixation. *Phytochemistry* 10, 1239–1244.
- Buckland, R. J., Watt, D. L., Chittoor, B., Nilsson, A. K., Kunkel, T. A., and Chabes, A. (2014). Increased and imbalanced dNTP pools symmetrically promote both leading and lagging strand replication infidelity. *PLoS Genet.* 10:e1004846. doi: 10.1371/journal.pgen.1004846
- Cousins, A. B., Badger, M. R., and Von Caemmerer, S. (2008). C₄ photosynthetic isotope exchange in NAD-ME- and NADP-ME-type grasses. *J. Exp. Bot.* 59, 1695–1703. doi: 10.1093/jxb/ern001
- Ding, Z., Weissmann, S., Wang, M., Du, B., Huang, L., Wang, L., et al. (2015). Identification of photosynthesis-associated C₄ candidate genes through comparative leaf gradient transcriptome in multiple lineages of C₃ and C₄ Species. *PLoS One* 10:e0140629. doi: 10.1371/journal.pone.0140629
- Efroni, I., Han, S. K., Kim, H. J., Wu, M. F., Steiner, E., and Birnbaum, K. D. (2013). Regulation of leaf maturation by chromatin-mediated modulation of cytokinin responses. *Dev. Cell* 24, 438–445. doi: 10.1016/j.devcel.2013.01.019
- Elledge, S. J., and Davis, R. W. (1990). Two genes differentially regulated in the cell cycle and by DNA-damaging agents encode alternative regulatory subunits of ribonucleotide reductase. *Genes Dev.* 4, 740–751. doi: 10.1101/gad.4.5.740
- Ellims, P. H., Kao, A. Y., and Chabner, B. A. (1981). Deoxycytidylate deaminase purification and some properties of the enzyme isolated from human spleen. *J. Biol. Chem.* 256, 6335–6340.
- Fekih, R., Takagi, H., Tamiru, M., Abe, A., Natsume, S., Yaegashi, H., et al. (2013). MutMap plus: genetic mapping and mutant identification without crossing in rice. *PLoS One* 8:e68529. doi: 10.1371/journal.pone.0068529
- Garton, S., Knight, H., Warren, G. J., Knight, M. R., and Thorlby, G. J. (2007). Crinkled leaves 8 - a mutation in the large subunit of ribonucleotide reductase - leads to defects in leaf development and chloroplast division in *Arabidopsis thaliana*. *Plant J.* 50, 118–127. doi: 10.1111/j.1365-313X.2007.03035.x
- Gawel, D., Fijalkowska, I. J., Jonczyk, P., and Schaaper, R. M. (2014). Effect of dNTP pool alterations on fidelity of leading and lagging strand DNA replication in *E. coli*. *Mutat. Res.* 759, 22–28. doi: 10.1016/j.mrfmmm.2013.11.003
- Gu, X., and Li, W. H. (1994). A model for the correlation of mutation rate with GC content and the origin of GC-rich isochores. *J. Mol. Evol.* 38, 468–475. doi: 10.1007/BF00178846
- Guilfoyle, T. J., and Hagen, G. (2007). Auxin response factors. *Curr. Opin. Plant Biol.* 10, 453–460. doi: 10.1016/j.pbi.2007.08.014
- Heuvel, S., and Dyson, N. J. (2008). Conserved functions of the Prb and E2F families. *Nat. Rev. Mol. Cell Biol.* 9, 713–724. doi: 10.1038/nrm2469
- Horiguchi, G., Fujikura, U., Ferjani, A., Ishikawa, N., and Tsukaya, H. (2006). Large-scale histological analysis of leaf mutants using two simple leaf observation methods: identification of novel genetic pathways governing the size and shape of leaves. *Plant J.* 48, 638–644. doi: 10.1111/j.1365-313X.2006.02896.x
- Horiguchi, G., Kim, G. T., and Tsukaya, H. (2005). The transcription factor AtGRF5 and the transcription coactivator AN3 regulate cell proliferation in leaf primordia of *Arabidopsis thaliana*. *Plant J.* 43, 68–78. doi: 10.1111/j.1365-313X.2005.02429.x
- Hou, H. F., Liang, Y. H., Li, L. F., Su, X. D., and Dong, Y. H. (2008). Crystal structures of *Streptococcus mutans* 2'-deoxycytidylate deaminase and its complex with substrate analog and allosteric regulator dCTP center dot Mg²⁺. *J. Mol. Biol.* 377, 220–231. doi: 10.1016/j.jmb.2007.12.064
- Hu, H. Q., Wang, L. H., Wang, Q. Q., Jiao, L. Y., Hua, W. Q., and Zhou, Q. (2014). Photosynthesis, chlorophyll fluorescence, and chlorophyll content of soybean seedlings under combined stress of bisphenol A and cadmium. *Environ. Toxicol. Chem.* 33, 2455–2462. doi: 10.1002/etc.2720
- Huang, P., Studer, A. J., Schnable, J. C., Kellogg, E. A., and Brutnell, T. P. (2017). Cross species selection scans identify components of C₄ photosynthesis in the grasses. *J. Exp. Bot.* 68, 127–135. doi: 10.1093/jxb/erw256
- Jia, X., Zhang, Z., Liu, Y., Zhang, C., Shi, Y., Song, Y., et al. (2009). Development and genetic mapping of SSR markers in foxtail millet [*Setaria italica* (L.) P. Beauv.]. *Theor. Appl. Genet.* 118, 821–829. doi: 10.1007/s00122-008-0942-9
- Ke, P. Y., Kuo, Y. Y., Hu, C. M., and Chang, Z. F. (2005). Control of dTTP pool size by anaphase promoting complex/cyclosome is essential for the maintenance of genetic stability. *Genes Dev.* 19, 1920–1933. doi: 10.1101/gad.1322905
- Kim, J. H., Choi, D., and Kende, H. (2003). The AtGRF family of putative transcription factors is involved in leaf and cotyledon growth in *Arabidopsis*. *Plant J.* 36, 94–104. doi: 10.1046/j.1365-313X.2003.01862.x
- Kohalmi, S. E., Glatte, M., McIntosh, E. M., and Kunz, B. A. (1991). Mutational specificity of DNA precursor pool imbalances in yeast arising from deoxycytidylate deaminase deficiency or treatment with thymidylate. *J. Mol. Biol.* 220, 933–946. doi: 10.1016/0022-2836(91)90364-c
- Kumar, D., Abdulovic, A. L., Viberg, J., Nilsson, A. K., Kunkel, T. A., and Chabes, A. (2011). Mechanisms of mutagenesis in vivo due to imbalanced dNTP pools. *Nucleic Acids Res.* 39, 1360–1371. doi: 10.1093/nar/gkq829
- Kumar, D., Viberg, J., Nilsson, A. K., and Chabes, A. (2010). Highly mutagenic and severely imbalanced dNTP pools can escape detection by the S-phase checkpoint. *Nucleic Acids Res.* 38, 3975–3983. doi: 10.1093/nar/gkq128
- Leija, C., Rijo-Ferreira, F., Kinch, L. N., Grishin, N. V., Nischan, N., Kohler, J. J., et al. (2016). Pyrimidine Salvage enzymes are essential for de novo biosynthesis of deoxyuridine nucleotides in *Trypanosoma brucei*. *PLoS Pathog.* 12:e1006010. doi: 10.1371/journal.ppat.1006010
- Lichtenthaler, H. K. (1987). [34] Chlorophylls and carotenoids: pigments of photosynthetic biomembranes. *Methods Enzymol.* 148, 350–382. doi: 10.1016/0076-6879(87)48036-1
- Lim, P. O., Lee, I. C., Kim, J., Kim, H. J., Ryu, J. S., and Woo, H. R. (2010). Auxin response factor 2 (ARF2) plays a major role in regulating auxin-mediated leaf longevity. *J. Exp. Bot.* 61, 1419–1430. doi: 10.1093/jxb/erq010
- Lincker, F., Philipps, G., and Chaboute, M. E. (2004). UV-C response of the ribonucleotide reductase large subunit involves both E2F-mediated gene transcriptional regulation and protein subcellular relocation in tobacco cells. *Nucleic Acids Res.* 32, 1430–1438. doi: 10.1093/nar/gkh310
- Lin, Q., Wang, D., Dong, H., Gu, S., Cheng, Z., Gong, J., et al. (2012). Rice APC/C^{TE} controls tillering by mediating the degradation of MONOCULM 1. *Nat. Commun.* 3:752. doi: 10.1038/ncomms1716
- Magyar, Z., De Veylder, L., Atanassova, A., Bakó, L., Inzé, D., and Bögre, L. (2005). The role of the *Arabidopsis* E2FB transcription factor in regulating auxin-dependent cell division. *Plant Cell* 17, 2527–2541. doi: 10.1105/tpc.105.033761
- Martins, P. K., Mafra, V., De Souza, W. R., Ribeiro, A. P., Vinecky, F., Basso, M. F., et al. (2016). Selection of reliable reference genes for RT-qPCR analysis during developmental stages and abiotic stress in *Setaria viridis*. *Sci. Rep.* 6:28348. doi: 10.1038/srep28348

- Martin-Trillo, M., and Cubas, P. (2010). TCP genes: a family snapshot ten years later. *Trends Plant Sci.* 15, 31–39. doi: 10.1016/j.tplants.2009.11.003
- Marx, A., and Alian, A. (2015). The first crystal structure of a dTTP-bound deoxycytidylate deaminase validates and details the allosteric-inhibitor binding site. *J. Biol. Chem.* 290, 682–690. doi: 10.1074/jbc.M114.617720
- McIntosh, E. M., Gadsden, M. H., and Haynes, R. H. (1986). Transcription of genes encoding enzymes involved in DNA synthesis during the cell cycle of *Saccharomyces cerevisiae*. *Mol. Gen. Genet.* 204, 363–366. doi: 10.1007/BF00331011
- Niu, M., Wang, Y. H., Wang, C. M., Lyu, J., Wang, Y. L., Dong, H., et al. (2017). ALR encoding dCMP deaminase is critical for DNA damage repair, cell cycle progression and plant development in rice. *J. Exp. Bot.* 68, 5773–5786. doi: 10.1093/jxb/erx380
- Pyke, K. A., and Leech, R. M. (1994). A genetic analysis of chloroplast division and expansion in *Arabidopsis thaliana*. *Plant Physiol.* 104, 201–207. doi: 10.1104/pp.104.1.201
- Qin, R., Zeng, D. D., Liang, R., Yang, C. C., Akhter, D., Alamin, M., et al. (2017). Rice gene SDL/RNRS1, encoding the small subunit of ribonucleotide reductase, is required for chlorophyll synthesis and plant growth development. *Gene* 627, 351–362. doi: 10.1016/j.gene.2017.05.059
- Sanchez, A., Sharma, S., Rozenzhak, S., Roguev, A., Krogan, N. J., Chabes, A., et al. (2012). Replication fork collapse and genome instability in a deoxycytidylate deaminase mutant. *Mol. Cell. Biol.* 32, 4445–4454. doi: 10.1128/Mcb.01062-12
- Sarojram, R., Sappl, P. G., Goldshmidt, A., Efroni, I., Floyd, S. K., and Eshed, Y. (2010). Differentiating *Arabidopsis* shoots from leaves by combined YABBY activities. *Plant Cell* 22, 2113–2130. doi: 10.1105/tpc.110.075853
- Schelbert, S., Aubry, S., Burla, B., Agne, B., Kessler, F., and Krupinska, K. (2009). Pheophytin pheophorbide hydrolase (Pheophytinase) is involved in chlorophyll breakdown during leaf senescence in *Arabidopsis*. *Plant Cell* 24, 507–518. doi: 10.1105/tpc.108.064089
- Scortecci, J. F., Serrao, V. H. B., Cheleski, J., Torini, J. R., Romanello, L., Demarco, R., et al. (2017). Spectroscopic and calorimetric assays reveal dependence on dCTP and two metals ($Zn^{2+} + Mg^{2+}$) for enzymatic activity of *Schistosoma mansoni* deoxycytidylate (dCMP) deaminase. *Biochim. Biophys. Acta* 1865, 1326–1335. doi: 10.1016/j.bbapap.2017.07.015
- Siegfried, K. R., Eshed, Y., Baum, S. F., Otsuga, D., Drews, G. N., and Bowman, J. L. (1999). Members of the YABBY gene family specify abaxial cell fate in *Arabidopsis*. *Development* 126, 4117–4128.
- Stutz, S. S., Edwards, G. E., and Cousins, A. B. (2014). Single-cell C(4) photosynthesis: efficiency and acclimation of *Bienertia sinuspersici* to growth under low light. *New Phytol.* 202, 220–232. doi: 10.1111/nph.12648
- Wang, P., Kelly, S., Fouracre, J. P., and Langdale, J. A. (2013). Genome-wide transcript analysis of early maize leaf development reveals gene cohorts associated with the differentiation of C-4 Kranz anatomy. *Plant J.* 75, 656–670. doi: 10.1111/tpj.12229
- Wang, P., Khoshravesh, R., Karki, S., Tapia, R., Balahadia, C. P., and Bandyopadhyay, A. (2017). Re-creation of a key step in the evolutionary switch from C3 to C4 leaf anatomy. *Curr. Biol.* 27, 3278–3287. doi: 10.1016/j.cub.2017.09.040
- Wang, Y., Ren, Y., Zhou, K., Liu, L., Wang, J., Xu, Y., et al. (2017). *WHITE STRIPE LEAF4* encodes a novel P-Type PPR protein required for chloroplast biogenesis during early leaf development. *Front. Plant Sci.* 8:1116. doi: 10.3389/fpls.2017.01116
- Weiner, K. X., Weiner, R. S., Maley, F., and Maley, G. F. (1993). Primary structure of human deoxycytidylate deaminase and overexpression of its functional protein in *Escherichia coli*. *J. Biol. Chem.* 268, 12983–12989.
- Xiang, J., Tang, S., Zhi, H., Jia, G., Wang, H., and Diao, X. (2017). *Loose Panicle1* encoding a novel WRKY transcription factor, regulates panicle development, stem elongation, and seed size in foxtail millet [*Setaria italica* (L.) P. Beauv.]. *PLoS One* 12:e0178730. doi: 10.1371/journal.pone.0178730
- Xu, J., Deng, Y. W., Li, Q., Zhu, X. D., and He, Z. H. (2014). *STRIPE2* encodes a putative dCMP deaminase that plays an important role in chloroplast development in rice. *J. Genet. Genomics* 41, 539–548. doi: 10.1016/j.jgg.2014.05.008
- Yoo, S. C., Cho, S. H., Sugimoto, H., Li, J. J., Kusumi, K., Koh, H. J., et al. (2009). Rice *Virescent3* and *Stripe1* encoding the large and small subunits of ribonucleotide reductase are required for chloroplast biogenesis during early leaf development. *Plant Physiol.* 150, 388–401. doi: 10.1104/pp.109.136648
- Zhang, S., Tang, C. J., Zhao, Q., Li, J., Yang, L. F., Qie, L. F., et al. (2014). Development of highly polymorphic simple sequence repeat markers using genome-wide microsatellite variant analysis in Foxtail millet [*Setaria italica* (L.) P. Beauv.]. *BMC Genomics* 15:78. doi: 10.1186/1471-2164-15-78

Conflict of Interest Statement: The authors declare that the research was conducted in the absence of any commercial or financial relationships that could be construed as a potential conflict of interest.

Copyright © 2018 Zhang, Tang, Tang, Luo, Jia, Zhi and Diao. This is an open-access article distributed under the terms of the Creative Commons Attribution License (CC BY). The use, distribution or reproduction in other forums is permitted, provided the original author(s) and the copyright owner(s) are credited and that the original publication in this journal is cited, in accordance with accepted academic practice. No use, distribution or reproduction is permitted which does not comply with these terms.